Sixth International Symposium on Marine Propulsors
smp'19, Rome, Italy, May 2019

Generation and propagation of noise from cavitating marine propellers

Kostas Belibassakis, Gerasimos Politis

School of Naval Architecture & Marine Engineering, National Technical University of Athens, Greece

ABSTRACT

Commercial ships contribute significantly to the background noise in the sea, and propeller is considered a main source concerning shipping noise. International Organisations have recently issued guidelines for the reduction of underwater noise from commercial shipping in order to address adverse impacts on marine life, including technical guidelines for the designers, shipbuilders and ship operators to minimize underwater radiated noise from ships. In this work, the development of an unsteady propeller analysis BEM is presented and discussed, providing us with the basic information and data that are subsequently used to estimate noise generation and propagation in the sea environment. The acoustic prediction is based on the time-dependent pressure and cavitation volume data that are used for the solution of FW-H equation by means of the Farassat formulation. The model is further elaborated to include the reflective effects of nearby boundaries of free surface (Lloyd mirror effect) and from the ship hull, which are expected to influence the sound directivity characteristics. Focusing on the estimation of shipping noise in the low frequency band of the spectrum, the applicability of the above noise generation models, in conjunction with suitable underwater acoustic propagation models, is subsequently discussed, for the estimation of the acoustic noise footprint from many sources representing the travelling ships in an examined geographical region.

Key words: propeller noise, unsteady load, cavitation, directivity effects, boundary effects

1. Introduction

Commercial ships contribute significantly to the background noise in the sea. This is due to the fact that the number, size and speed of ships continuously increase leading to increasing noise levels. Various studies, covering the period 1950-2007, indicate strong relationship between commercial shipping activity and global economic growth (Frisk 2012). Furthermore, the importance of shipping noise and its impact on marine environment is also demonstrated by the fact that at low frequencies (below 300 Hz), ambient noise levels have been increased by 15-20 dB over the last century (Wittekind et al. 2014, McKenna et al. 2012). On the side of mitigation measures, IMO has recently issued guidelines for the reduction of underwater noise from commercial shipping to address adverse impacts on marine life, including technical guidelines for the designers, shipbuilders and ship operators to minimize underwater radiated noise from ships (IMO 2014).

The broad bandwidth of the produced noise spectrum indicates that shipping is a complex noise source composed by the superimposition of several contributors. The propeller noise is considered as main contributor to commercial shipping noise, especially under cavitating conditions, whereas, below cavitation inception on-board machinery and hydrodynamic noise due to wave-structure interaction and wave breaking are also important. Generally, propeller noise is dominant at high speeds. As for the flow-induced noise due to ship-hull hydrodynamic interactions it is considered to be negligible far from the vessel (AQUO 2015).

In this work, underwater noise spectrum induced by marine propellers is estimated using a numerical model. The prediction of unsteady performance of marine propellers with and without cavitation is based on a numerical lifting surface theory, which provide us with the basic information and data that are subsequently exploited to study noise generation. In general, the acoustic prediction is based on the time-dependent pressure and sheet cavity volume data that are used as input for the Farassat formulation (Farassat 2001) of the FW-H equation (Ffowcks Williams & Hawkings, 1969). For the numerical formulation of noise prediction in the low-frequency band a simplified model based on appropriate contributions of acoustic monopoles and dipoles is derived. The unsteady sheet cavity volume fluctuations are modeled by monopole sources, whereas,

the fluctuations of the unsteady pressure jump on propeller blades are modeled by corresponding dipole terms. Having calculated the noise spectrum at any point near the sound source, the directivity patterns are obtained, indicating anisotropic characteristics. Subsequently, the present model is further elaborated to study the reflective effects of nearby boundaries of free surface (Lloyd mirror effect) and ship hull. It is shown that free-surface effects, strongly influence the underwater noise propagation in the marine environment comparatively to the omni-directional source assumption.

2. Unsteady propeller analysis

The propeller hydrodynamic analysis in inhomogeneous inflow conditions (ship's wake due to hull's boundary layer) is based on a vortex lattice method (Kerwin & Lee, 1978, Lee 1979). Given the induced unsteadiness due to ship wake and propeller's rotating motion, a time-stepping method is applied for the solution. The complete propeller discretization is obtained by a vortex lattice consisted of quadrilateral vortex element on the mean camber sufaces; see Fig.1. The method is modified in order to include blade thickness and sheet cavitation effects by including source-sink distribution with appropriate density.

To account for the effects of trailing vorticity, a free vortex sheet downstream of the blades has been incorporated to the model. Since the geometry of this additional boundary is unknown, it has to be determined as part of the solution. This is usually accomplished by free wake analysis, based on a wake relaxation method to incorporate the nonlinear effects. Taking into consideration the unsteadiness of the problem, the grid representing the free wake surface is forced to dynamically evolve with time; see, e.g., Politis (2004). According to this method some initial wake geometry is assumed for which wake grid panels are defined. However, assuming that the shape of hydrodynamic trailing vortex sheets can be defined by means of wake model, the problem can be approximately reduced to an integral equation over the solid surface coupled with the Kutta condition, which substantially accelerates the numerical solution.

In the case of wake models the radial distribution of the hydrodynamic pitch angle, are selected to be given by a simplified formula, in terms of the main geometrical and hydrodynamic parameters; see, e.g., Lee (1979), Politis & Belibasakis, (1990). Within the transition wake region, trailing vortex lines emanate from the trailing edge of each blade aligned to the local trailing edge angle bisector.

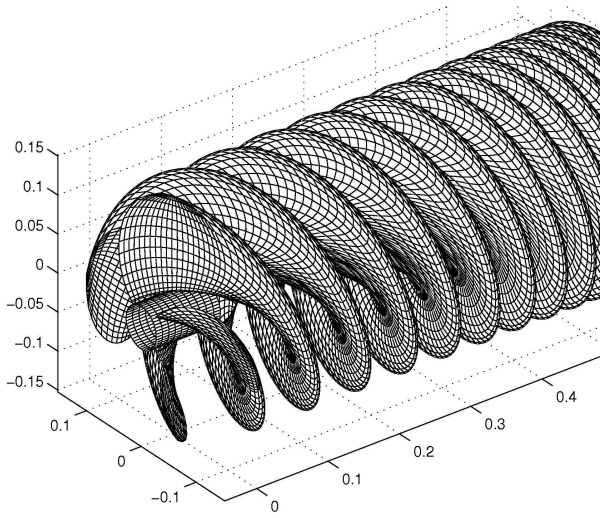

Figure 1. Representation of propeler blades and trailing vortex sheets using vortex elements on the mean camber surface.

Subsequently, moving in the downstream direction, the trailing vortex lines gradually deform to smoothly match the ultimate wake trailing vortex lines. In the case of the deformed wake model an additional contraction of the blade wake is superimposed; see Fig.1.

2.1 Boundary Value Problem

The propeller blades are considered to be a set of symmetrically arranged thin blades, rotating with a constant angular velocity about a common axis in an unbounded, incompressible fluid. The symmetric arrangement along with the hypothesis of weak interaction between the blades, are exploited in order to reduce the computational cost. The presence of extraneous boundaries such as the rudder, the hub and the ship hull, are neglected, except that the last is recognized as the body generating the non-uniform flow field (ship's wake). The blade boundary layer and shed vortex wake thickness is assumed to be thin so that the fluid rotation due to the propeller is confined in a thin layer.

For the incoming velocity field, it is also assumed the smallness of angle of attack, as well as the smallness of spatial variation. The propeller approximately treated by separating the velocity field in two terms: the first one refers to the rotational wake, whereas the second to perturbation velocity due to the existence of propeller. The last can be considered irrotational outside the blade boundary layer. Under these considerations, the Euler equations can be numerically integrated, giving us a decoupled formulation for the velocity and pressure fields (Belibasakis & Politis 1998).

The principle of conservation of mass is the governing equation throughout the fluid encompassing the blades, the shed wake, and the cavity. The total fluid velocity $\mathbf{w}$ in the propeller frame of reference is given by:

$$\mathbf{w} = \mathbf{U} + \mathbf{A} + \boldsymbol{\Omega} \times \mathbf{x} + \mathbf{u}, \quad \mathbf{u} = \nabla \Phi , \tag{1}$$

where $\mathbf{U}$ and $\boldsymbol{\Omega}$ are propeller translational and rotational speed, respectively, $\mathbf{A}$ denotes the ship's wake, and $\mathbf{u}$ is the propeller's disturbance velocity field. The latter is obtained as solution of the Laplace equation for the disturbance flow potential outside the propeller blades and trailing vortex sheets, as well as the cavity surface:

$$\nabla^2 \Phi = 0 . \tag{2}$$

The unknown disturbance potential is numerically approximated by imposing the following boundary conditions in order to form a close set of equations:

2.1.1 Tangency condition on the blade surface

In a blade-fixed coordinate system rotating with the propeller, the impermeability condition on the blade and solid surfaces is described as:

$$\mathbf{n}\mathbf{w} = 0 , \tag{3}$$

where, $\mathbf{n}$ is the vector normal to the blade surface. Using the following representation for the disturbance velocity field:

$$\mathbf{u}(\mathbf{x}_0) = \frac{1}{4\pi} \int_{S_B \cup S_C} \frac{\sigma \mathbf{r}}{r^3} dS(\mathbf{x}) + \frac{1}{4\pi} \int_{S_B \cup S_W} \boldsymbol{\gamma} \times \frac{\mathbf{r}}{r^3} dS(\mathbf{x}), \tag{4}$$

where, $\mathbf{r} = \mathbf{x}_0 - \mathbf{x}$, σ is surface source-sink distribution defined by means of Eq.(3) on the blade and cavity surface, and $\boldsymbol{\gamma}$ the surface vorticity on the blade and wake surface; see Fig.2. In the Vortex Lattice method the continuous distributions of source-sink and vorticity are modelled by discrete source-sinks and vortices. Using Eq.(4) in the boundary condition Eq.(3), it results in a linear algebraic system from which the discrete singularities on the propeller blades are calculated. The above representation ensures the satisfaction of condition at infinity at each time step, in the form of demanding the vanishing of the perturbation velocity at large distances from the propeller.

2.1.2 Kutta condition at the trailing edge

In the case of ideal flow, Kutta condition prevents the existence of infinite velocities at the trailing edge. In the present study, necessitating equal pressure (dynamic Kutta condition) as the trailing edge is approached from both sides of the blade surface and provides us information concerning the vorticity field on the blade wake in terms of the solution of the integral equation in previous time steps.

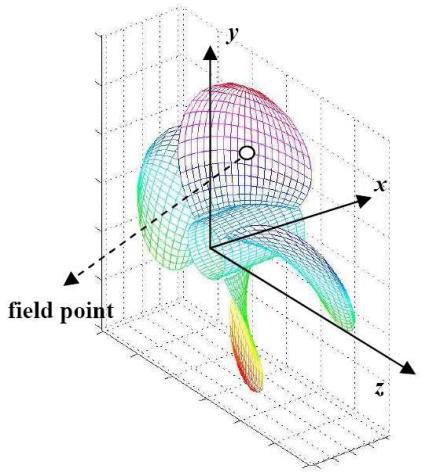

Figure 2. Representation of propeler blades and trailing vortex sheets using vortex and source-sink elements on the mean camber surface.

More, specifically, a relation is obtained for the spanwise shed vorticity from the trailing edge of the blade in the trailing vortex sheets, in terms of the temporal variation of the circulation around the blade section at each spanwise position, consistent with Kelvin's theorem for the conservation of circulation.

2.1.3 Conditions on the trailing vortex sheets

The velocity jump across each trailing vortex sheet is tangential to these surfaces (kinematic condition), and the pressure is continuous across this blade wake (dynamic condition). The latter are approximately satisfied by propagating the vorticity emitted at the trailing edge to each blade wake model.

2.2 Numerical solution scheme

The propeller hydrodynamic problem is solved at each time step, and the singularity distributions are calculated, from which velocity is computed using Eqs.(1) and (4). Once the velocities are found, the pressure distribution is obtained from Bernoulli's equation, as follows:

$$\frac{p - p^{(I)}}{\rho} = -\frac{\partial \Phi}{\partial t} - \frac{1}{2}\left(|\boldsymbol{w}|^2 - |\boldsymbol{q} + \boldsymbol{A}|^2 \right) = 0, \tag{5}$$

where, $p^{(I)}$ denotes the incident field pressure in the moving coordinate system fixed to the propeller and ρ is the density of the water; see also Belibassakis & Politis (1998). For operation at specific value of the advance coefficient:

$$J = \frac{U + A_m}{nD} , \tag{6}$$

where, $U + A_m$ is the mean value of the propeller inflow at its disc, n the propeller revolutions per minute

and $D = 2R$ is the propeller diameter, the unsteady forces and moments, including thrust and torque, are subsequently calculated by pressure integration on propeller blades. The results concerning the thrust and toque coefficients are obtained as follows:

$$K_T = \frac{T}{\rho n^2 D^4} \quad \text{and} \quad K_Q = \frac{Q}{\rho n^2 D^5} . \tag{7}$$

The corresponding coefficients corresponding to each symmetrical part (each blade) of the propeller are dented as $K_{T,1}$ and $K_{Q,1}$, respectively.

3. Propeller blade cavitation

In the case of cavitating flow, the prescribed vapor pressure provides an additional criterion that controls the cavity formation and decay. Some important phenomena such as general cavity inception and surface tension are not considered. It is assumed that the cavity starts at the leading edge of the blade, and that only the suction side of the blade is cavitating (Lee, 1979, Kinnas & Young 2003). The non-dimensional parameters which characterize the cavitating flow field are the cavitation and Froude numbers, defined on the basis of the propeller rotational speed (n) as follows:

$$\sigma_n = \frac{p - p_v}{0.5\rho n^2 D^2} , \quad \text{and} \quad F_n = \frac{n^2 D}{g} , \tag{8}$$

where, p is the atmospheric and hydrostatic pressure at the propeller shaft center, p_v denotes the vapour pressure and g the gravity acceleration.

3.1 Conditions on cavitating propeller

The problem concerning the unknown disturbance velocity and potential in the case of cavitating propeller is solved by imposing additional boundary conditions due to the presence of the cavity. Introducing a curvilinear coordinate system (u^1, u^2, u^3) as shown in Fig.3, and denoting by $h(u^1, u^2, t)$ the thickness of the cavity normal to the blade surface at the point (u^1, u^2) at time *t*, the Kinematic Boundary Condition (KBC) is used to determine the position of the cavity surface, given by the following equation:

$$\frac{D}{Dt}\left[u^3 - h(u^1, u^2, t)\right] = 0 , \tag{9}$$

where, the material derivative appearing in the above equation is formulated in terms of the total flow velocity on the surface of the cavity. Moreover, the Dynamic

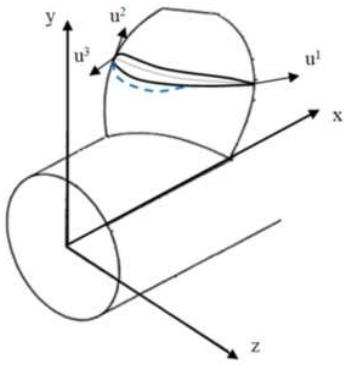

Figure 3. Calculation of cavity surface on the suction side at each section of the propeller blade.

Boundary Condition (DBC) requires that the pressure, which is calculated using Bernoulli's equation (5), everywhere inside the cavity volume to be constant and equal to the given cavity pressure:

$$p = p_c . \tag{10}$$

3.2 Numerical solution of the cavitating problem

The cavity boundary is determined by an iterative process in which the dynamic boundary condition is satisfied on an approximate cavity surface and the kinematic boundary condition is used to update the surface. In the first iteration, the panels representing the cavity are placed on the foil surface. In subsequent iterations, the cavity surface is updated using the kinematic condition, and the boundary elements are moved to the updated surface. The local cavity length $\ell(u^2, t)$, defined as the arc length of the projection of the cavity (on the nose-tail axis along u^1) at each radial position $u^2 = const$ is determined from the following requirement (closure condition) at each spanwise strip:

$$h(u^1 = \ell(u^1, t), u^2, t) = 0 . \tag{11}$$

For a given cavitation number σ_n, the above requirement is used as the basis of an iterative solution scheme to calculate the cavity's boundary and its temporal variation. As an example of application we consider two 5-bladed model propellers, one without skew (KP068) and one with 70deg skew (KP070) for which detailed experimental data are available in (Kim et al. 1988). The basic dimensions are: *D*=0.25m, *P/D*=1.2 (at 70% of tip radius), expanded area ratio 72.5%. The propellers operate in an axial wake, as shown in Fig.4. In this case, the operating condition concerning the advance coefficient is *J*=0.889. Moreover, in the experiments the Froude number is $F_n = 10.45$ and the cavitation number is $\sigma_n = 3$.

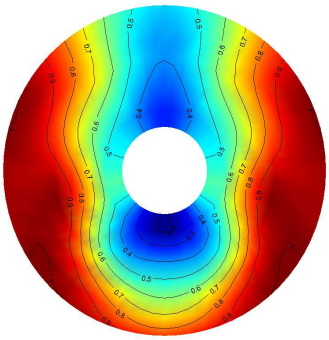

Figure 4. Distribution of axial wake (Kim et al. 1988) on the propeller disc.

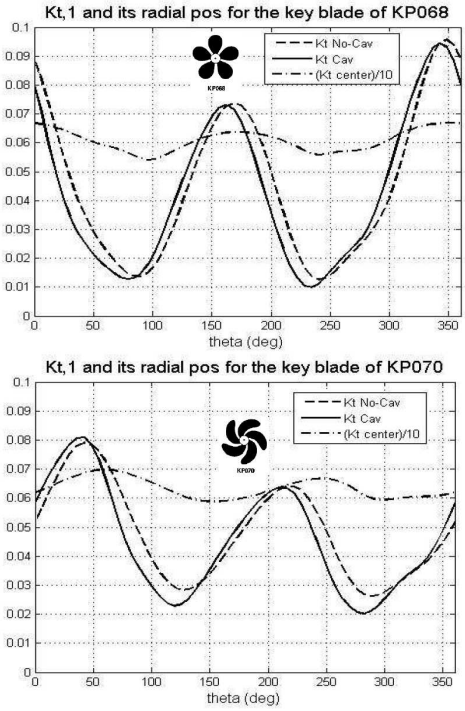

Figure 5. Circumferential variations of $K_{t,1}$ and radial coordinate of center of blade thrust for the normal KP068 and skewed KP070 propellers. The solid and dashed lines represent the cavitating and non-cavitating conditions, respectively.

The calculated results of unsteady hydrodynamic analysis for the non-cavitating and cavitating conditions are presented in Figs.5 and 6. In particular, Fig.5 shows the circumferential variation of blade thrust coefficient for the key blade ($K_{t,1}$). Dashed lines indicate the non-cavitating conditions and solid lines the effect of cavitation. In the same plots, it also presented the radial position of the thrust center in terms of the propeller radius (multiplied by 0.1). In Fig.6 the calculated cavitation pattern on the blades of skewed propeller KP070 in the wake of Fig.4 is presented, for various angular positions. Also, the blade cavity volume and the coordinates of its center are shown. For comparison in Fig. 6(b) the calculated result concerning the cavity volume of the unskewed propeller KP068, as calculated by the present method, is also presented by using red lines.

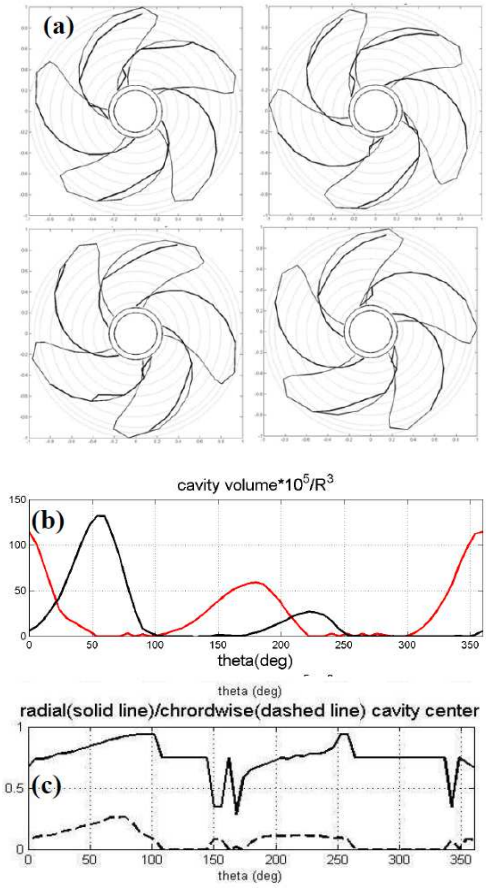

Figure 6. (a) Calculated cavitation pattern on the blades of propeller KP070 in the wake of Fig.4, for various angular positions. (b) Key blade cavity volume and (c) center of volume, respectively, as predicted by the present model.

In general, the present method predictions are found in good agreement with measured data (see Kim et al. 1988).

4. Propeller noise prediction model

As propeller rotates in the non-uniform wake, it is subjected to unsteady pressure loads and cavitation which lead to discrete tonal and increased broadband noise (Seol et al. 2005). Low frequency noise is caused by the fluctuations of blade pressure and variation of unsteady sheet cavitation volume. The former has dipole character-istics and the latter is modelled by a bubble that acts as an acoustic monopole. High-frequency noise is caused by sheet cavity collapse and/or by shock wave generation.

The formulation of Lighthill's acoustic analogy proposed by Ffowcs, Williams and Hawkings (1969) is:

$$\frac{1}{c^2}\frac{\partial^2 p'}{\partial t^2} - \nabla^2 p' = g_m + g_d + g_q \,, \qquad (12)$$

where p' denotes the acoustic pressure, c is the speed of sound in the medium (c=1500 to 1550m/s for water). The various terms in the right-hand side correspond to forcing from the acoustic monopole, dipole and quadrupole

source terms (Farassat & Myers,1988), defined as follows:

$$g_m = \frac{\partial}{\partial t}\left[\rho u_n \,|\nabla f|\,\delta(f)\right],\quad g_d = -\frac{\partial}{\partial x_i}\left[l_i\,|\nabla f|\,\delta(f)\right], \quad (13)$$

$$g_q = -\frac{\partial^2}{\partial x_i \partial x_j}\left[T_{ij} H(f)\right], \quad (14)$$

where, f=0 indicates the moving surfaces u_n the corresponding normal velocity, l_i the loads, T_{ij} is the Lighthill's stress tensor and H denotes the Heaviside function. The quadrupole term is important for strongly transonic flow phenomena manifested at higher frequencies. Given that the speed of sound in water is much greater than the flow velocities, and focusing on the low-frequency part of the generated noise spectrum the contributions by the latter term are neglected in the present work. In the sequel Farassat formulation 1A (Farassat 2001, Seol et al. 2005) is employed offering an integral representation of the solution of Eq.(12) forced only by the monopole and dipole terms. The acoustic pressure field is accordingly given by thickness and loading components, as follows:

$$p'(\mathbf{x}_0,t) = p'_T(\mathbf{x}_0,t) + p'_L(\mathbf{x}_0,t)\ . \quad (15)$$

The loading term is given by:

$$4\pi p'_L(\mathbf{x}_0,t) = -\frac{1}{c}\frac{d}{dt}\int_{f=0}\left[\frac{[\![p]\!]\mathbf{n}\hat{r}}{r(1-M_r)}\right]_{ret} dS + \int_{f=0}\left[\frac{[\![p]\!]\mathbf{n}\hat{r}}{r^2(1-M_r)}\right]_{ret} dS\ , \quad (16)$$

where $[\![p]\!]$ denotes the pressure jump on the blade surface, M_r denotes Mach number in the r-direction and the integrand is calculated at retarded time. For relatively large distances (of the order of several propeller diameters) of the observation point from the propeller, we use the following leading-order approximation:

$$r = |\mathbf{x}_0 - \mathbf{x}| \approx |\mathbf{x}_0 - \mathbf{x}_{T,k}(t)|,\ \text{and}\ \hat{r} \approx (\mathbf{x}_0 - \mathbf{x}_{T,k}(t))/r\ , \quad (17)$$

where, $\mathbf{x}_{T,k}(t)$ denotes the center of thrust on the k-blade, which is the most important load on the lifting surface. Using the fact that the Mach number is very small, Eq.(17) eventually leads to the following simplification:

$$p'_L(\mathbf{x}_0,t) \approx -\frac{1}{4\pi c}\sum_{k=1}^{Z}\frac{d\tilde{T}_k(t_r)}{dt}\frac{x_P - x_{T,k}(t_r)}{r_{T,k}^{\ 2}} + \frac{1}{4\pi}\sum_{k=1}^{Z}\tilde{T}_k(t_r)\frac{x_P - x_{T,k}(t_r)}{r_{T,k}^{\ 3}}\ , \quad (18)$$

where $\tilde{T}_k(t_r)$ denotes the fluctuating part of the k-blade thrust, as e.g. shown in the first subplots of Fig.5 for propellers KP069 and KP070, and $t_r = r/c$ denotes the retarded time which represents the time which is needed for the acoustic wave to travel between the observation point $\mathbf{x}_0$ and the disturbance generating point $\mathbf{x}_{T,k}$. Similarly, for the thickness effect we have:

$$4\pi p'_T(\mathbf{x}_0,t) = \rho\frac{\partial}{\partial t}\int_{f=0}\left[\frac{u_n}{r(1-M_r)}\right]_{ret} dS. \quad (19)$$

Considering the same approximations, the above equation is simplified in the following form:

$$4\pi p'_T(\mathbf{x}_0,t) \approx \frac{\rho}{r}\frac{\partial}{\partial t}\int_{f=0}[u_n]_{ret} dS\ . \quad (20)$$

Moreover, we consider that the blades are very thin in comparison to the cavity volume, and using:

$$\int_{f=0} u_n dS \approx \frac{dQ_c(t)}{dt}, \quad (21)$$

where $Q_c(t)$ denotes the calculated cavity volume, as e.g. shown in the first subplots of Fig.5, we finally obtain:

$$p'_T(\mathbf{x}_0,t) \approx \frac{\rho}{4\pi}\sum_{k=1}^{Z}\frac{d^2Q_{c,k}(t_r)}{dt^2}\frac{1}{r_{c,k}},\quad r_{c,k} = |\mathbf{x}_0 - \mathbf{x}_{Q,k}(t_r)|, \quad (22)$$

where $\mathbf{x}_{Q,k}(t)$ denotes the center of cavity volume of the k-blade.

5. Results and discussion

The predictive capability of the above simplified model is indicated by rescaling the KP060 and KP070 propellers from model to full scale (D=7m, n=100rpm, and U=20.2kn), simulating a real case scenario of a container ship. What is more, we assume a moving observer with exactly the same forward speed as propeller's one. The selected observation point is set equal to 10 times the propeller radius (R) in order to satisfy the model's simplifications to be valid. Initially, it is taken on the propeller shaft axis and the calculation is exploited in a spectral analysis so as to derive and compare the noise frequency spectra.

Calculations based on the above approximate formulas, Eqs. (18) and (22), significantly reduce the computational cost of the surface integrals (16) and (19), respectively. Numerical results are presented in Fig.7 for the normal (KP060) and skewed (KP070) propellers. More specifically, in these figures the frequency spectrum of loading term (dipole) for the non-cavitating (dashed lines) and cavitating (solid lines) conditions is shown, with reference to 1μPa/Hz^2 at 35m. We observe the appearance of a peak at the blade frequency, which is sharper in the case of the skewed propeller. It is seen that without cavitation (dashed lines) the noise is reduced in the case of skewed propeller. However, under cavitating conditions, an increase of the peak of the noise spectrum for the skewed propeller is observed, which is due to the increased volume as calculated by the present model (see Fig.6b).

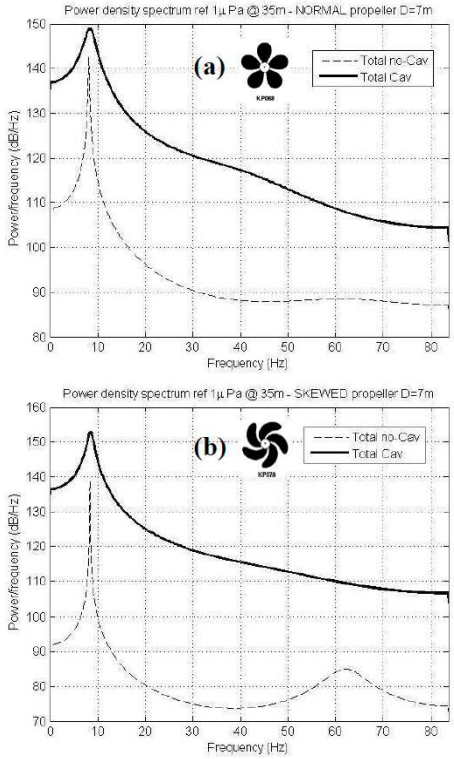

Figure 7. Power density spectrum for the cavitating and non-cavitating cases of propeller KP068 and KP070 with reference to 1μPa at 35m.

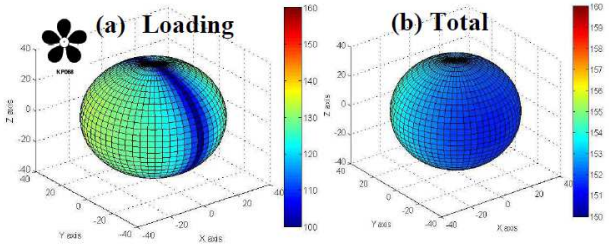

Figure 8. Noise directivity 3D contours of cavitating KP068 due to: (a) loading and (b) total noise.

Also, it is evident that cavitation significantly modifies (of the order of 20dB/Hz) the levels of the acoustic spectral density. It is also seen that the loading term of KP070 propeller presents a second peak around the 65Hz, which is due to the phase difference between the two terms of the loading noise. Furthermore, the directivity characteristics of the noise are presented in Fig.8 in the case of the normal propeller. As expected the loading term has clear dipole characteristics, while the total noise directivity pattern is more regular and mostly affected by the manifestation of blade cavitation. Similar patterns are also obtained concerning the skewed propeller. Given the fact that most studies report noise results at the distance of 1m from the propeller, and taking into consideration that the total noise directivity pattern is close to omni-directional, and assuming homogeneous acoustic parameters in the vicinity of the propeller, the present results can been rescaled to a distance of 1m by using the standard geometrical

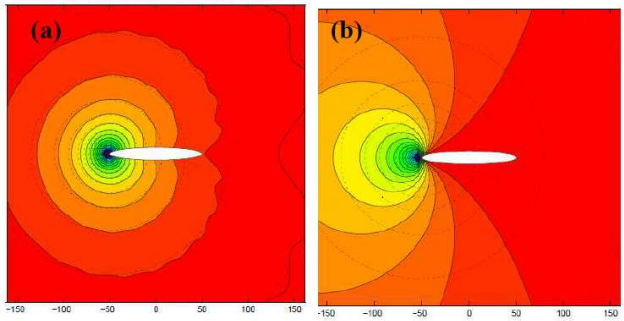

Figure 9. Modification of the directivity characteristics of the acoustic field due to presence of: (a) hard hull boundary (Neumman b.c.) and (b) soft hull (Dirichlet b.c.)

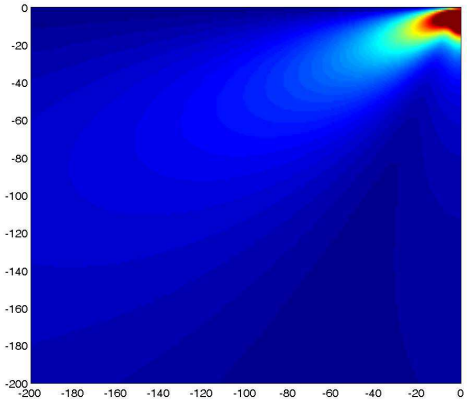

Figure 10. Modification of the directivity characteristics of the acoustic field on the vertical plane due to the free-surface effect.

spreading law concerning the transmission losses:

$$\mathrm{TL}[\mathrm{dB\ re\ 1\mu Pa\ @\ 1m}] = 20\log r\ . \qquad (23)$$

The present model can be further elaborated to include the effects of additional boundaries. As an example, the effect of hull boundary on the directivity characteristics of the noise generated by the propeller is shown in Fig.9. In particular, we consider a simple (monopole) harmonic source representing the propeller located at the shaft axis (near the frequency corresponding to the center of the second octave band), and an obstacle representing the hull (L=100m and B=15m). Numerical results are presented modeling the hull surface as an ideal hard surface (Neumann b.c.) in Fig.9(a) and as soft surface (Dirichlet b.c.) in Fig.9(b), respectively. In reality, the effect of the hull is defined by the reflective characteristics of the surface (dependent on the material, stiffness, coating, surface roughness etc) and is expected to be more close to the hard boundary condition (shown in Fig.9a), indicating that the modification of the directivity pattern of the propeller due to the hull is rather small. On the other hand, the effect of free surface due to Lloyd mirror effect by a pressure release boundary (zero acoustic pressure on the free surface) is important, as shown in Fig.10, for the same as before frequency. The latter effect can be easily incorporated in the present simplified model by mirroring

the acoustic monopoles and dipoles of each propeller blade above the horizontal plane, leading to the following expression:

$$p'_L(\mathbf{x}_0,t) \approx -\frac{1}{4\pi c}\sum_{k=1}^{Z}\frac{d\tilde{T}_k(t_r)}{dt}\frac{x_P - x_{T,k}(t_r)}{r_{T,k}^{\ 2} - \tilde{r}_{T,k}^{\ 2}} + \frac{1}{4\pi}\sum_{k=1}^{Z}\tilde{T}_k(t_r)\frac{x_P - x_{T,k}(t_r)}{r_{T,k}^{\ 3} - \tilde{r}_{T,k}^{\ 3}} \quad , \tag{24}$$

$$p'_T(\mathbf{x}_0,t) \approx \frac{\rho}{4\pi}\sum_{k=1}^{Z}\frac{d^2Q_{c,k}(t_r)}{dt^2}\left(\frac{1}{r_{c,k}} - \frac{1}{\tilde{r}_{c,k}}\right), \tag{25}$$

where $\tilde{r}_{T,k}$, $\tilde{r}_{c,k}$ denote the distances from the image points of the centers of thrust and cavity volume of each *k*-blade above the free surface, respectively.

6. Conclusions

A numerical model is developed for the prediction of noise generated from cavitating or non-cavitating marine propellers operating in unsteady inflow conditions in the wake of the ship. The hydrodynamic part is analyzed by a velocity-based vortex lattice method, providing the unsteady pressure on the blades and cavitation data. The latter are subsequently used, in conjunction with Farassat formulation, to calculate acoustic radiation from moving surfaces and predict the acoustic spectrum at a distance of several diameters from the propeller, representing the source of marine propeller noise. An approximate model is derived, exploiting information and integrated data concerning the time history of blade sheet cavity volume and the unsteady blade thrust. The latter are used to calculate the monopole and dipole forcing terms of the acoustic equation and derive the propeller acoustic spectrum in the low and moderate frequency band. Also, the directivity characteristics of the propeller noise are calculated, and the effect of nearby boundaries on underwater noise propagation are presented comparatively to the omnidirectional source assumption. In particular, the effect of the free surface as a pressure release boundary (Lloyd mirror effect), and of the ship hull, treated as hard and soft boundary, are illustrated. Future work will include the validation of present method concerning the noise prediction by comparison against available data (e.g., Sharma et al. 1990 and similar).

References

AQUO (2015). Report R2.9, Ship Underwater Radiated Noise Patterns, Achieve Quieter Oceans by shipping noise footprint reduction (FP7 Project No314227).

Belibasakis, K.A., Politis, G.K. (1998). 'A non-linear velocity based Boundary Element Method for the analysis of marine propellers in unsteady flow'. International Shipbuilding Progress **45** 93-133.

Farassat, F. , Myers, M.K., (1988). 'Extensions of Kirchhoff's formula to radiation from moving surfaces'. Journal of Sound and Vibration **123** , 451–460.

Farassat, F., (2001). 'Acoustic radiation deom rotating blades – the Kirchhoff method in aeroacousics'. Journal of Sound and Vibration **239** 785-800.

Ffowcs Williams J.E., Hawkings, D.L., (1969). 'Sound generated by turbulence and surfaces in arbitrary motion'. Philosophical Transactions of the Royal Society **A 264**.

Frisk, G. (2012). 'Noiseconomics: The relationship between ambient noise levels in the sea and global economic trends'. Scient. Rep. 2, Art.: 437.

IMO (2014). Guidelines for the Reduction of Underwater Noise from Commercial Shipping to Address Adverse Impacts on Marine Life – non mandatory technical advices, International Maritime Organization MEPC.1/Circ.833.

Kerwin, J., Lee, C.S., (1978). ,Prediction of steady and unsteady performance of marine propellers by numerical lifting surface theory'. SNAME Trans. 86.

Kim, K.H. , Nguyen, P.H., (1988). 'Propeller cavitationa and cavitation induced pressure fluctuation: Comparison between theory and experiments'. Proc. SNAME propellers'88 Symposium (Virginia Beach).

Kinnas, S., Young, Y.L., (2003). 'Modeling of Unsteady Sheet Cavitation on Marine Propeller Blades'. Intern. J. of Rotating Machinery **9**, 263–277.

Lee, C.S., (1979). 'Prediction of Steady Unsteady Performa-nce of Marine Propellers With or Without Cavitation by Numerical Lifting Surface Theory'. PhD Thesis, MIT, Department of Ocean Engineering

Lighthill, M.J. (1952). 'On sound generated aerodynamically, 1. General Theory'. Proceedings of the Royal Society **A211**, 564–587.

McKenna, M.F., Ross, D., Wiggins, S.M., Hildebrand, J.A., (2012). 'Underwater radiated noise from modern commercial ships'. J. Acoust. Soc. Am. 131 92-103.

Politis, G.K., (2004). 'Simulation of unsteady motion of a propeller in a fluid including free wake modeling'. Engin. Analysis with Boundary Elements **28**, 633–53.

Politis, G.K., Belibasakis, K.A., (1990). 'Application of Panel Methods to Linearized Lifting Surface Propeller Performance Problem', Proc. 5th Intern Congress on Marine Technology, IMAEM'90, Athens, Greece.

Seol, H., Suh, J.C., Lee, S., (2005). 'Development of hybrid method for the prediction of underwater propeller noise'. Journal of Sound and Vibration **288**, 345–360.

Sharma S., Mani K., Arakeri V. (1990). 'Cavitation noise studies onmarine propellers'. Journal of Sound and Vibration **138**, 255–283.

Wittekind, D., Schuster, M., (2014). 'Propeller Cavitation Noise and Background Noise in the Sea'. Proc. 1st Intern. Meeting – Prop. Noise & Vibr. 6-7 Nov. 2014, Istanbul.